iScience

CellPress
OPEN ACCESS

Article

The BASP1 transcriptional corepressor modifies chromatin through lipid-dependent and lipid-independent mechanisms

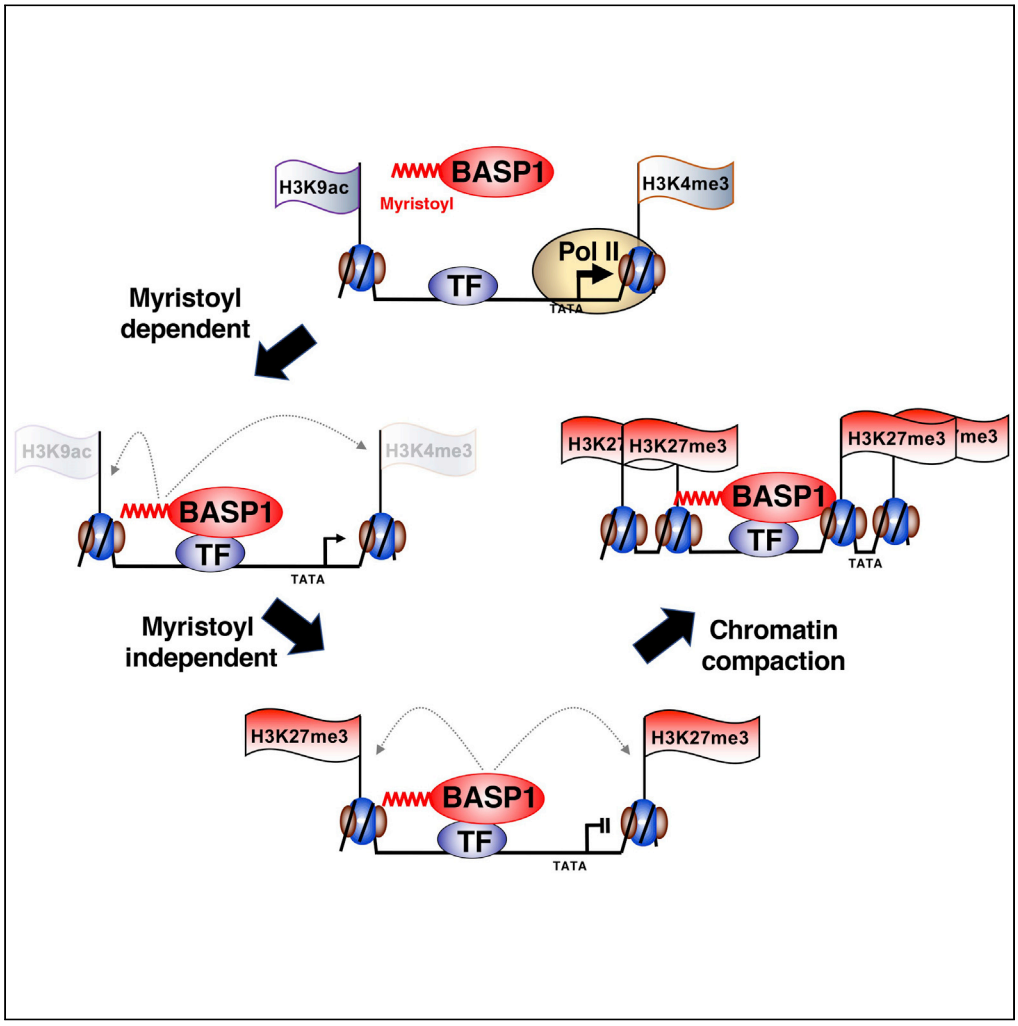

Alexander J. Moorhouse, Amy E. Loats, Kathryn F. Medler, Stefan G.E. Roberts

stefan.roberts@bristol.ac.uk

Highlights

Myristoylation of BASP1 is required to remove active H3K9ac and H3K4me3

BASP1-dependent placement of H3K27me3 does not require the myristoylation of BASP1

The tumor suppressor activity of BASP1 is myristoylation dependent

Lipidation of BASP1 modulates chromatin accessibility

Moorhouse et al., iScience 25, 104796
August 19, 2022
https://doi.org/10.1016/j.isci.2022.104796

iScience

CellPress
OPEN ACCESS

Article

The BASP1 transcriptional corepressor modifies chromatin through lipid-dependent and lipid-independent mechanisms

Alexander J. Moorhouse,[1] Amy E. Loats,[1] Kathryn F. Medler,[2] and Stefan G.E. Roberts[1,2,3,*]

SUMMARY

The transcriptional corepressor BASP1 requires N-terminal myristoylation for its activity and functions through interactions with nuclear lipids. Here we determine the role of BASP1 lipidation in histone modification and the modulation of chromatin accessibility. We find that the removal of the active histone modifications H3K9ac and H3K4me3 by BASP1 requires the N-terminal myristoylation of BASP1. In contrast, the placement of the repressive histone modification, H3K27me3, by BASP1 does not require BASP1 lipidation. RNA-seq and ATAC-seq analysis finds that BASP1 regulates the activity of multiple transcription factors and induces extensive changes in chromatin accessibility. We find that ~50% of BASP1 target genes show lipidation-dependent chromatin compaction and transcriptional repression. Our results suggest that BASP1 elicits both lipid-dependent and lipid-independent functions in histone modification and transcriptional repression. In accordance with this, we find that the tumor suppressor activity of BASP1 is also partially dependent on its myristoylation.

INTRODUCTION

BASP1 was initially identified as a cytoplasmic signaling protein in neuronal cells (Mosevitsky, 2005) but has since been found to be widely expressed and localized to the nucleus in several cell types via a canonical nuclear localization sequence (Carpenter et al., 2004; Goodfellow et al., 2011; Toska and Roberts, 2014). A role for BASP1 in transcriptional regulation was first identified as a cofactor for the Wilms' tumor one protein WT1 (Carpenter et al., 2004). BASP1 binds to WT1 and converts it from a transcriptional activator to a repressor. BASP1 has subsequently been found to act as a repressive cofactor for other transcriptional regulators including MYC (Hartl et al., 2009), ERα (Marsh et al., 2017), and YY1 (Santiago et al., 2021), suggesting that it is broadly deployed in transcription control (Hartl and Schneider, 2019). Our understanding of how BASP1 regulates transcription is limited and has, to date, largely been studied as a transcriptional corepressor of WT1.

BASP1 is N-terminally myristoylated and we demonstrated that this lipid motif is required for its function as a transcriptional repressor (Toska et al., 2012, 2014). BASP1 also contains a consensus cholesterol binding motif adjacent to the myristoyl moiety (Epand, 2008). Indeed, both phosphatidylinositol 4,5-bisphosphate (PIP_2) and cholesterol are recruited to promoter regions and are required for transcriptional repression by BASP1 (Toska et al., 2012, 2014; Loats et al., 2021). The myristoylation of BASP1 is required for interaction with both PIP_2 and cholesterol (Toska et al., 2012; Loats et al., 2021). PIP_2 assists in the recruitment of HDAC1 to mediate the deacetylation of histone H3K9 and direct transcriptional repression (Toska et al., 2012).

Several studies have demonstrated that BASP1 acts as a tumor suppressor, for example in hepatocellular carcinoma (Tsunedomi et al., 2010), gastric cancer (Li et al., 2020), and breast cancer (Marsh et al., 2017). Consistent with its tumor suppressor activity, BASP1 has a role in maintaining the differentiated state and is required to maintain the functional differentiated state of taste receptor cells in mice (Gao et al., 2014, 2019). BASP1 can also block the transformation of fibroblasts by v-myc (Hartl et al., 2009). Moreover, BASP1 interferes with the action of the Yamanaka proteins in the induction of pluripotent stem cells by repressing WT1 target genes (Blanchard et al., 2017). Taken together, current studies suggest that BASP1 plays a major role in the maintenance of the differentiated state through the modulation of the function of several transcriptional activator proteins.

[1]School of Cellular and Molecular Medicine, University of Bristol, Bristol BS8 1TD, UK

[2]Department of Biological Sciences, University at Buffalo, Buffalo, NY 14260, USA

[3]Lead contact

*Correspondence: stefan.roberts@bristol.ac.uk

https://doi.org/10.1016/j.isci.2022.104796

The mechanism of action of BASP1 as a transcription cofactor is poorly understood, but its physiological activities suggest extensive roles in gene regulation. In this study, we set out to determine how BASP1 regulates transcription through histone modifications and the roles of the myristoyl motif of BASP1. We find that the lipidation of BASP1 plays a selective role in its action as a transcription cofactor and is required for specific histone modification leading to the modulation of the chromatin environment in order to elicit specific transcriptional effects. Our results suggest that BASP1 plays a widespread role in regulating the chromatin environment and transcription control.

RESULTS

BASP1 mediates the removal of active histone modifications and the placement of repressive H3K27me3

K562 cells express endogenous WT1 but do not express BASP1 (Goodfellow et al., 2011). As we have shown before, the introduction of BASP1 into K562 cells (B-K562 cells) leads to the transcriptional repression of the WT1 target genes AREG and VDR compared to the control K562 cells (V-K562 cells; Figure 1A; Goodfellow et al., 2011; Toska et al., 2012, 2014; Loats et al., 2021). We next performed chromatin immunoprecipitation (ChIP) to detect WT1, BASP1, and a selection of specific histone modifications at the promoter regions of the WT1 target genes AREG and VDR (Figure 1B). WT1 was present at the promoter region of the AREG and VDR genes in both control V-K562 cells and B-K562 cells, while BASP1 was present at the promoter region only in B-K562 cells. Analysis of H3K9ac and H3K4me3, indicators of transcriptionally active promoter regions, demonstrated that these histone modifications are removed when BASP1 is recruited to the promoter in B-K562 cells and the genes are transcriptionally repressed. These data are consistent with our previous studies of BASP1 function in histone modification (Toska et al., 2012; Loats et al., 2021). We also analyzed the H3K27me3 histone modification associated with transcriptional repression. We found that BASP1 induces the trimethylation of H3K27 at both the AREG and VDR promoter regions. Taken together, these results demonstrate that BASP1 functions by both the removal of active histone modifications (H3K9ac and H3K4me3) and the placement of the repressive histone mark H3K27me3.

We have previously used a conditional BASP1 mouse to demonstrate that BASP1 transcriptionally represses the WT1 target genes LEF1 and PTCH1 in taste receptor cells (Gao et al., 2014, 2019). A floxed BASP1 mouse was crossed with a Krt8-Cre-ER mouse to delete BASP1 in the fully differentiated Krt8-expressing taste cells. We used this model to perform ChIP to analyze BASP1-dependent histone modifications at the LEF1 and PTCH1 promoters in taste receptor cells. Consistent with our previous studies, knockout of BASP1 expression in taste cells leads to the upregulation of LEF1 and PTCH1 expression (Figure 1C). ChIP analysis confirmed that WT1 was present in the promoter region of the LEF1 and PTCH1 genes in both the control and BASP1 KO taste cells while BASP1 was only present in the promoter regions in the taste receptor cells from control mice (Figure 1D). Analysis of H3K9ac, H3K4me3, and H3K27me3 demonstrated that loss of BASP1 leads to the accumulation of the active histone modifications H3K9ac and H3K4me3, and the removal of the H3K27me3 repressive modification. These findings, using an *in-vivo* model of BASP1 function, confirm and extend our analysis in K562 cells demonstrating that BASP1 directs the removal of the active histone modifications H3K9ac and H3K4me3 and the placement of repressive H3K27me3.

Myristoylated BASP1 is recruited to gene promoters

Our previous work demonstrated that the mutation BASP1-G2A, which prevents N-terminal myristoylation of BASP1, leads to loss of transcriptional repression function (Toska et al., 2012, 2014). Although total cellular BASP1 is stoichiometrically N-terminally myristoylated (Mosevitsky, 2005), it has not yet been demonstrated that this lipidated form of BASP1 is present within the nucleus and is directly recruited to gene promoter regions. We, therefore, used a click chemistry approach to analyze the myristoylation status of nuclear BASP1 in K562 cell line derivatives. V-K562 and B-K562 cells along with G-K562 cells (expressing BASP1-G2A) were incubated in lipid-free media supplemented with myristic acid alkyne that is utilized by cells as a substrate for N-terminal myristoylation (Wright et al., 2015). Nuclei were then prepared as we described before using a method that avoids contamination with either ER or Golgi complex (Loats et al., 2021). Using click chemistry, the alkyne-myristoyl moiety was crosslinked to azide-PEG3-biotin which was then detected using a streptavidin-linked fluorophore. BASP1 was simultaneously probed using immunocytochemistry. In control V-K562 cells, myristoyl was detected within the purified nuclei of K562 cells and was particularly evident at the nuclear membrane (Figure 2A). This staining pattern is consistent with the known N-terminal myristoylation of lamins (Linde and Stick, 2010). In B-K562 cells there was similar staining at the nuclear periphery and also enhanced intranuclear staining. BASP1-G2A showed reduced

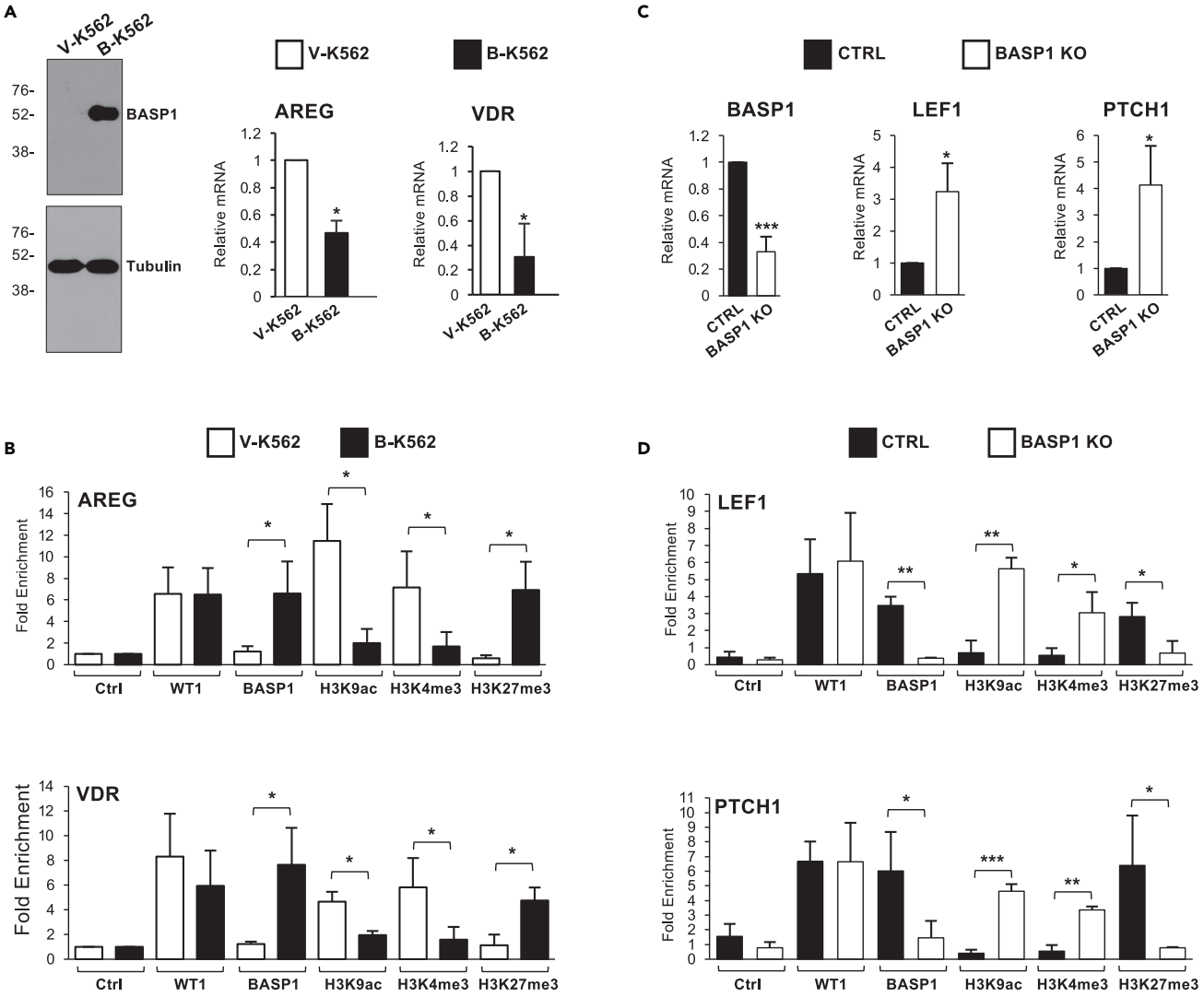

Figure 1. BASP1 directs the removal of active histone modifications H3K9ac and H3K4me3 and the placement of repressive H3K27 trimethylation

(A) Immunoblotting of extracts prepared from V-K562 and B-K562 cells to confirm BASP1 expression. β-tubulin immunoblotting was performed as a loading control. Molecular weight markers are shown at left (kDa). cDNA was prepared from V-K562 cells and B-K562 cells and expression of AREG and VDR was quantitated relative to GAPDH. Data are SD from the mean (SDM) for three independent experiments. * = $p < 0.05$ by students t-test.

(B) V-K562 or B-K562 cells were subjected to chromatin immunoprecipitation (ChIP) with control (ctrl) antibodies or antibodies against WT1, BASP1 or the histone modifications indicated. Data are presented as fold-enrichment over a control genomic region and error bars are SDM of three independent experiments. * = $p < 0.05$ by students t-test.

(C) Krt8-BASP1-CRE mice were treated with tamoxifen for 8 days and then 7 days later taste buds were isolated and RNA prepared. cDNA was then used to monitor the expression of BASP1, LEF1, and PTCH1 compared to GAPDH. Error bars are SDM for three independent experiments. * = $p < 0.05$ by students t-test.

(D) Mice were treated as in part C but isolated taste cells were subjected to chromatin immunoprecipitation with the antibodies indicated. Error bars are SDM for three independent experiments. * = $p < 0.05$, ** = $p < 0.01$ and *** = $p < 0.005$ by students t-test.

colocalization with myristoyl compared to wtBASP1 (Pearson quantitation of the proportion of BASP1 signal that overlaps with myristoyl is shown in Figure 2B).

We next used click chemistry combined with immunoprecipitation to determine the association between BASP1 and nuclear myristoyl. V-K562, B-K562, and G-K562 cells were cultured in the presence of myristic acid alkyne as above for 48 h and, following the click chemistry reaction with azide-PEG3-biotin, nuclear protein extracts were prepared then immunoprecipitation was performed with streptavidin-coated beads. wtBASP1, but not BASP1-G2A, co-immunoprecipitated with the alkyne-myristoyl (Figure 2C). We have previously combined click chemistry with ChIP (Click-ChIP; Loats et al., 2021) and therefore used this technique

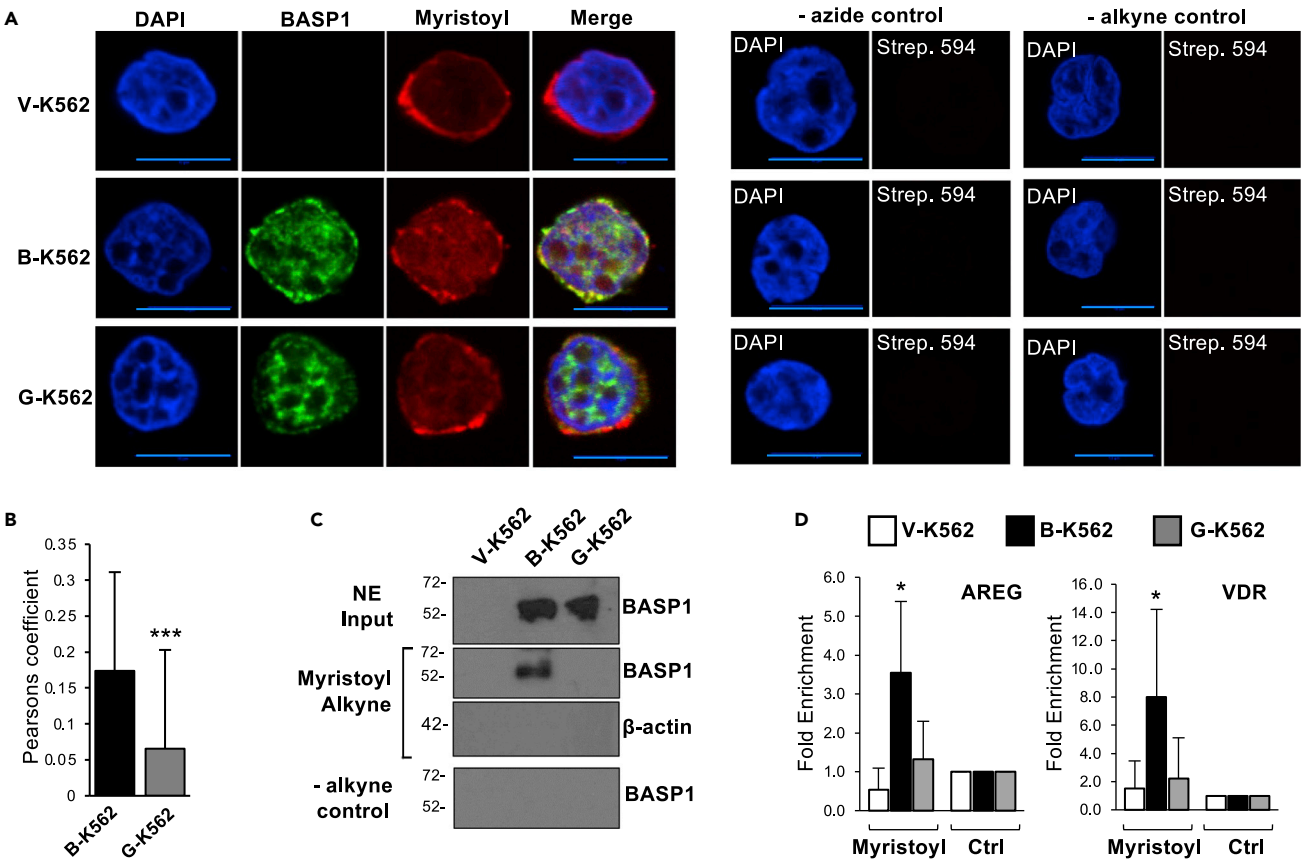

Figure 2. Myristoylated BASP1 is present in the nucleus and is recruited to the promoter regions of WT1 target genes

(A) The indicated cell lines were incubated in lipid-free media in the presence of 10 μg/mL myristic acid alkyne for 20 h. Nuclei were prepared and incubated with azide PEG3-biotin, then the click reaction was initiated using 2mM $CuBF_4$. Immunohistochemistry was then performed with streptavidin-linked antibodies (Myristoyl) and BASP1 antibodies. Scale bar (blue) is 10μm. Control assays were performed that lacked azide PEG3-biotin (-azide control) or myristic acid alkyne (-alykyne control) and are shown at right.

(B) Quantification of the colocalization of BASP1 and Myristoyl in B-K562 and G-K562 nuclei was analyzed using Pearson's correlation coefficient. *** = $p < 0.005$ following students t-test comparing Pearson's values from BK and GK nuclei over three independent experiments ($n = 67$).

(C) V-K562, B-K562, and G-K562 cells were incubated with ethanol (-alkyne control) or 10 μg/mL alkyne-Myristic acid as above and subjected to a click chemistry reaction. Nuclear extracts were prepared and precipitation was performed with streptavidin beads. Immunoblotting was then performed with either BASP1 antibodies or control β-actin antibodies. Molecular weight marker in kDa shown to left of each blot. Gels are representative of three independent experiments.

(D) The cell line derivatives were treated in part A and following the click chemistry reaction, ChIP was performed with either streptavidin-linked beads (Myristoyl) or control beads (Ctrl). Data are shown as fold enrichment of Myristoyl at the AREG and VDR promoters in V-K562, B-K562, and G-K562 cells compared to the alkyne-free control precipitation. Error bars are SDM of ten independent experiments with * = $p < 0.05$ by student's t test comparing B-K562 or G-K562 with control cell line V-K562.

to determine if myristoyl is recruited to the promoter region of WT1 target genes. We found that myristoyl associates with the AREG and VDR promoters at a significantly increased level when wtBASP1 is also present at the promoter (Figure 2D; compare V-K562 with B-K562), but at a reduced level in K562 cells that express BASP1-G2A (G-K562). Our previous study (confirmed in Figure 3B) demonstrated that BASP1 G2A is recruited to gene promoters at a level equivalent to wtBASP1 (Toska et al., 2012, 2014). These data demonstrate that the detection of myristoyl in the promoter region of WT1 target genes is dependent on BASP1 and that this association requires an intact G2 target site of myristoylation in BASP1.

Myristoylation of BASP1 is required for the removal of active chromatin modifications but not for the placement of repressive H3K27me3

Our data so far have demonstrated that myristoylated BASP1 is present at the promoter region of WT1 target genes. Our previous work (Toska et al., 2012, 2014), confirmed in Figures 3A and 3B, has shown

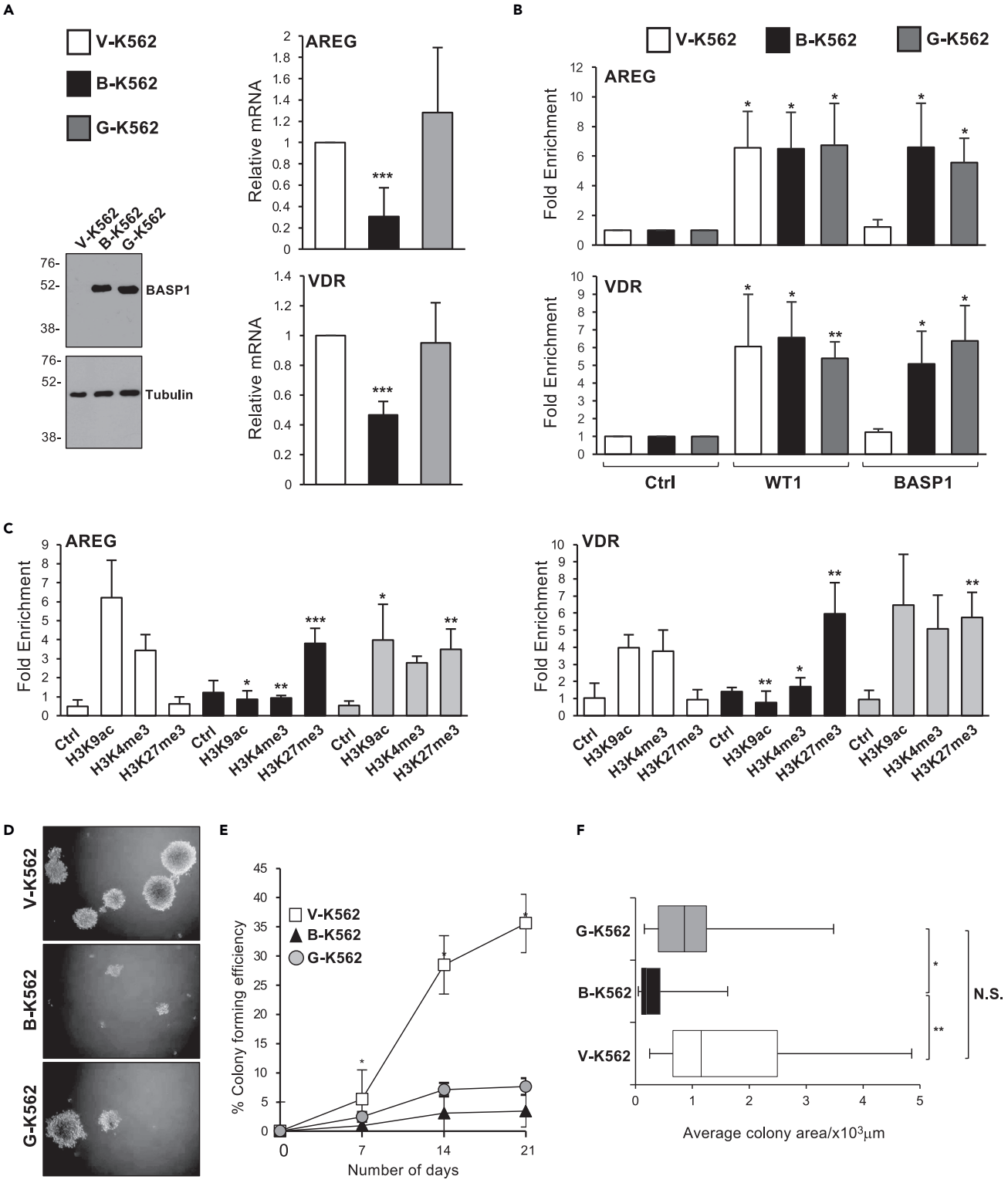

Figure 3. The role of myristoylation of BASP1 in transcription, histone modification, and tumorigenesis

(A) Expression of the WT1 target genes AREG and VDR was monitored relative to GAPDH in V-K562, B-K562, and G-K562 cells. Immunoblotting was performed to confirm the expression of the BASP1 derivatives.

Figure 3. *Continued*

(B) V-K562, B-K562, and G-K562 cells were subjected to ChIP analysis with antibodies against WT1, BASP1, or control. Data are presented as mean fold enrichment with SDM (from three independent experiments) at the AREG and VDR promoters compared to a control genomic region. Students t-test, * = $p < 0.05$, ** = $p < 0.005$.

(C) V-K562, B-K562, and G-K562 cells were subjected to ChIP analysis with antibodies against H3K9ac, H3K4me3, H3K27me3, or control. Data are presented as mean fold enrichment with SDM (from three independent experiments) at the AREG and VDR promoters compared to a control genomic region. Students t-test, * = $p < 0.05$, ** = $p < 0.005$, *** = $p < 0.001$.

(D) Representative images (from three independent experiments) of V-K562, B-K562, and G-K562 cells seeded into agar dishes for 21 days.

(E) Colony formation efficiency was assessed on days 7, 14, and 21 for V-K562, B-K562, and G-K562 cells. Error bars are SDM of three independent experiments.

(F) Box and Whisker plot of average colony area after 21 days growth of V-K562, B-K562, and G-K562 cells in agar. * = $p < 0.05$, ** = $p < 0.005$, n.s. (no significant difference) by student's t-test comparing three independent experiments.

that BASP1-G2A lacks transcriptional corepressor activity despite being recruited along with WT1 to the promoter region of WT1 target genes. We demonstrated before that BASP1-G2A is defective in the deacetylation of H3K9 (Toska et al., 2012). We, therefore, tested if BASP1-G2A was able to mediate the demethylation of H3K4me3 or the placement of repressive H3K27me3. ChIP analysis confirmed that BASP1-G2A was defective in the removal of the active H3K9ac mark (Figure 3C). We also found that BASP1-G2A was defective in the removal of H3K4me3. Thus, myristoylation of BASP1 is required for the removal of active histone modifications. In contrast, BASP1-G2A was still able to support the placement of repressive H3K27me3 at both the AREG and VDR promoters. Thus, the N-terminal myristoylation of BASP1 is required to mediate the removal of the active histone modifications, but is not required to place the repressive H3K27me3 modification. These findings suggest a dual mechanism of lipidation-dependent and lipidation-independent transcriptional repression by BASP1.

Myristoylation of BASP1 plays a role in the tumor suppressor activity of BASP1

BASP1 acts as a tumor suppressor in several cell types and slows the growth of K562 cells (Goodfellow et al., 2011; Toska et al., 2014). We, therefore, tested the effects of wtBASP1 and BASP1-G2A on the formation of anchorage-independent colonies of K562 cells in soft agar assays (Figure 3D). The number of V-K562, B-K562, and G-K562 colonies greater than 50 cells in size were counted over a three-week period (Figure 3E). Expression of wtBASP1 led to a significant decrease in the colony-forming ability of K562 cells. Measurement of the average area of colonies revealed that, as well as forming fewer colonies, B-K562 cells form significantly smaller colonies (Figure 3F). Expression of BASP1-G2A also led to a significant decrease in the colony-forming ability of K562 cells (Figure 3E). However, the average area of G-K562 colonies did not significantly differ from that of V-K562 colonies (Figure 3F). Thus, myristoylation of BASP1 is not required to suppress the formation of anchorage-independent colonies but contributes to inhibiting the growth of the established colonies. We conclude that the myristoylation of BASP1 plays a partial role in its tumor suppressor function in K562 cells.

Genome-wide analysis of the requirement for BASP1 myristoylation in transcriptional repression

Our results so far demonstrate that BASP1 directs histone modifications that are both dependent (H3K9 deacetylation and H3K4 demethylation) and independent (H3K27 methylation) on the N-terminal myristoylation of BASP1. In addition, myristoylation of BASP1 is partially required for its tumor suppressor activity. Taken together, these findings suggest that non-myristoylated BASP1 is likely to retain partial activity in transcriptional regulation that we have not observed here or before (Toska et al., 2012, 2014) in targeted gene analysis. We, therefore, determined the gene expression profiles of B-K562, G-K562, and control V-K562 cells using RNA-seq. Comparing the data from V-K562 and B-K562 cells (Figure 4A) supports our previous genome-wide analysis with 3064 genes regulated by BASP1 (2165 genes repressed and 899 genes activated; Table S1; Goodfellow et al., 2011). As before, the majority of the known WT1 target genes that show altered expression were transcriptionally repressed (70.3% of the 105 WT1 target genes that changed significantly (padj 0.05); Goodfellow et al., 2011; Figures 4B and 4C). Our data further show that BASP1-G2A is partially defective in transcriptional repression when compared to wtBASP1, repressing 58.8% of the genes that are repressed by wtBASP1 (Figure 4A). This was reduced to 45.7% when considering only WT1 target genes (Figures 4B and 4D). In fact, BASP1-G2A activated many of the target genes that are repressed by wtBASP1 (Figure 4D).

Pathway enrichment analysis of genes repressed by wtBASP1 reveals several networks (canonical pathways and upstream regulators) that are enriched for significantly repressed differentially expressed genes in

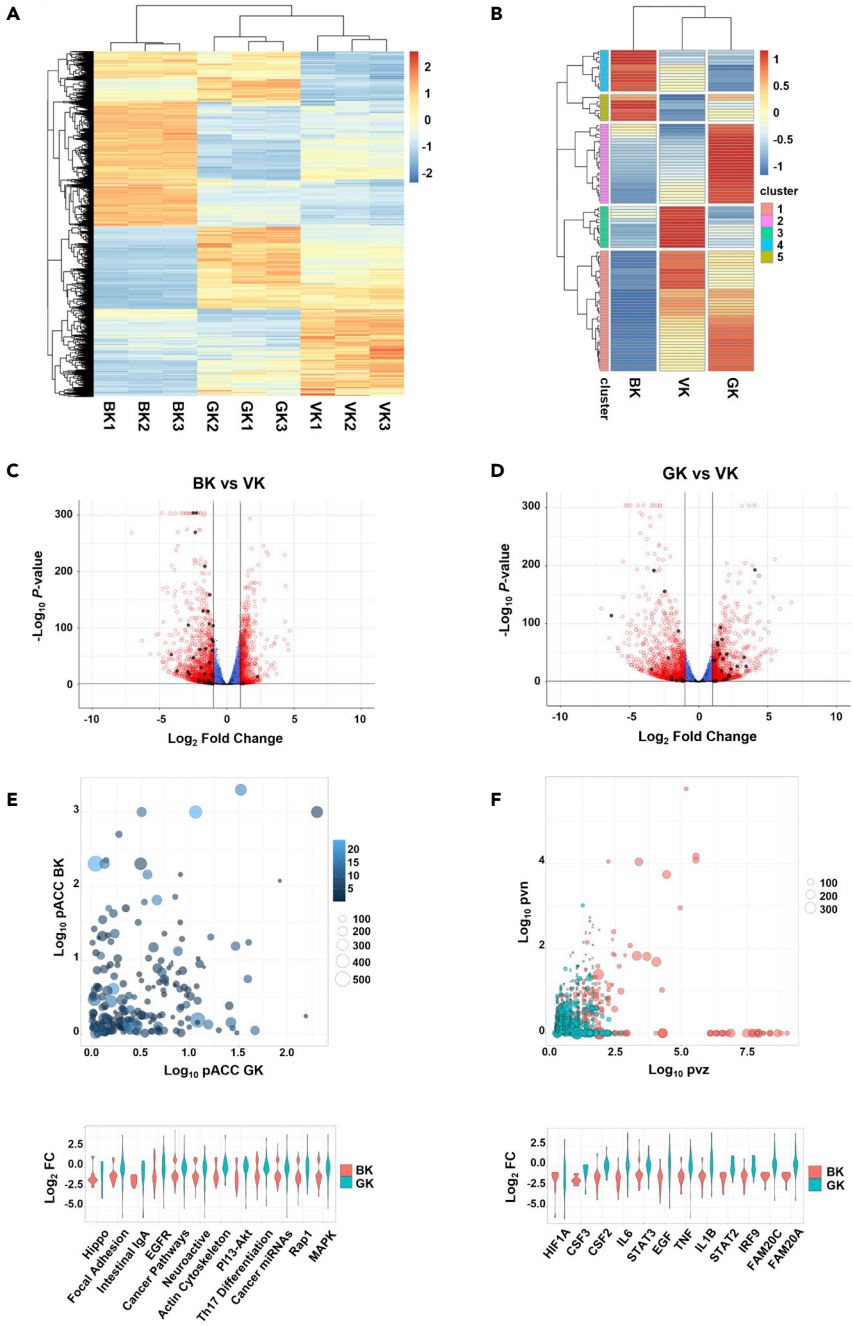

Figure 4. BASP1 elicits lipidation-dependent and lipidation-independent transcriptional regulation

(A) Gene expression is shown for genes at padj ≤0.05 and fold-change ≥ 1 for BK vs VK for all genes. Data from three independent RNAseq experiments for V-K562, B-K562, and G-K562 cells is shown. See Table S1 (Quality control analysis of RNA-seq and ATAC-seq data).

(B) As in part A but only analysis of known WT1 target genes is shown. Signals are the average of three independent RNAseq experiments.

(C) Differential gene expression is shown in volcano plots for B-K562 cells vs V-K562 cells. WT1 target genes are shown in black.

(D) As in part C but comparing V-K562 cells with G-K562 cells.

(E) Differentially regulated gene networks are plotted for BK and GK, compared with VK: Canonical pathways are positioned by -Log10 perturbation accumulation (pAcc) for B-K562 cells (y axis) and for G-K562 cells (x axis). Pathways are

Figure 4. *Continued*
sized by the number of genes in each pathway and colored by pathway over-representation (pORA) for B-K562 cells vs V-K562 cells.
(F) Upstream regulators inhibited in B-K-562 cells are positioned by -Log10 p values for the number of targets consistent with inhibition (pvn) and regulator *Z* score (pvz), and balloons are sized by the total number of target genes for each regulator. The following thresholds were applied to E: -Log10 pAcc ≥2, -Log10 pvn ≥1.5, and to F: -Log10 pvz ≥2.5, violin plots are ordered left to right by -Log10 pAcc and, -Log10 pvz, respectively and show fold-change values for those networks in B-K562 cells and G-K562 cells, vs V-K562 cells. See also Figure S1.

B-K562 cells, and further demonstrate their derepression in G-K562 cells (Figures 4E and 4F). We also identified other networks downregulated in B-K562, but not G-K562 cells, including those involved in the response to the H3K27 Demethylase Inhibitor GSK-J4, the selective estrogen receptor modulator Tamoxifen, the extra-cellular space, and pre-ribosome cellular processes (Figure S1A). Together these data show the repressive effects of wtBASP1 are partially lost with the BASP1-G2A mutant derivative, specifically, the BASP1-dependent downregulation of transcription factors, upstream regulators, drug responses, and canonical pathways genome-wide (Figures 4E, 4F, and S1A). BASP1 was also found to regulate the function of a number of transcription factors, in particular MYC, RELA, TFCP2, POU3F2, YY1, and CTCF (Figure S1B; note that the expression level of the transcription factors was unchanged by wtBASP1 or BASP1 G2A compared to control cells). In the case of MYC, the effect of wtBASP1 was both activation and repression and a similar profile for MYC target genes was observed with K562 cells expressing BASP1-G2A. In contrast, wtBASP1 was predominantly repressive at RELA, TFCPP2, POU3F2, YY1, and CTCF target genes but BASP1-G2A elicited transcriptional activation at most genes that changed expression. Taken together the data in Figure 4 demonstrate that the myristoylation of BASP1 is required for its transcriptional repressor function at ~50% of target genes. Furthermore, BASP1 regulates the expression of the target genes of both previously described BASP1-associated transcription factors (MYC, YY1, CTCF) and newly identified targets.

The effects of BASP1 and requirement for myristoylation on the chromatin landscape

Our targeted ChIP analysis of histone modifications (Figures 1 and 3) suggests that BASP1 likely makes extensive changes in the chromatin environment. Furthermore, the BASP1-G2A mutant derivative is defective in the removal of active chromatin modifications (H3K9ac and H3K4me3) but not the addition of repressive chromatin modification (H3K27me3). To investigate the effects of these BASP1-dependent chromatin remodeling events genome-wide, we conducted sequencing experiments to Assay for Transposase-Accessible Chromatin (ATAC-seq; Table S1). Comparing control V-K562 cells with B-K562 cells the data demonstrate that chromatin accessibility is substantially altered genome-wide by wtBASP1 with 79% of the peak changes in closed chromatin compared to 21% of the changes in open chromatin (Figure 5A). These data are consistent with broad transcriptional repression by BASP1. 15% of the peak changes were within the upstream regions and transcription start sites of genes, but there were also general BASP1-dependent changes across the gene bodies. When we compared the ATAC-seq data with the RNA-seq data, we observed a strong correlation between the BASP1-dependent formation of closed chromatin within the gene proximity and transcriptional repression of the associated gene by BASP1 (Figure 5B). Specifically, 514 genes that are transcriptionally repressed by BASP1 showed BASP1-dependent formation of closed chromatin peaks. Analysis of these genes by g:profiler highlighted several categories related to the physiological functions of BASP1 including developmental processes and cell differentiation (Figure S2A).

BASP1-G2A caused more peak changes in ATAC-Seq than wtBASP1 (Figure S2B), although the ratio of changes in open chromatin versus changes in closed chromatin was increased (Figure 4C). Direct comparison of wtBASP1 with BASP1-G2A showed that 66.3% of genes affected by wtBASP1 correlated with both decreased chromatin accessibility and increased transcriptional repression, while for BASP1-G2A, this only occurred for 45.5% of the genes (Figure 4D). Indeed, BASP1-G2A was either completely (Figure 4E, cluster 3) or partially (Figure 4E cluster 4) defective in inducing closed regions of chromatin at most genomic regions modified by wtBASP1 (Non-relative data are shown in Figure S2C). Thus, although BASP1-G2A showed a defect in driving closed chromatin at many of the sites acted upon by wtBASP1, it did not show an overall lower activity in driving the formation of closed chromatin. This is consistent with BASP1-G2A acting at several sites that are not regulated by wtBASP1. Figure S3A shows a pathway analysis demonstrating that wtBASP1 and BASP1 G2A regulate many genes involved in distinct cellular processes.

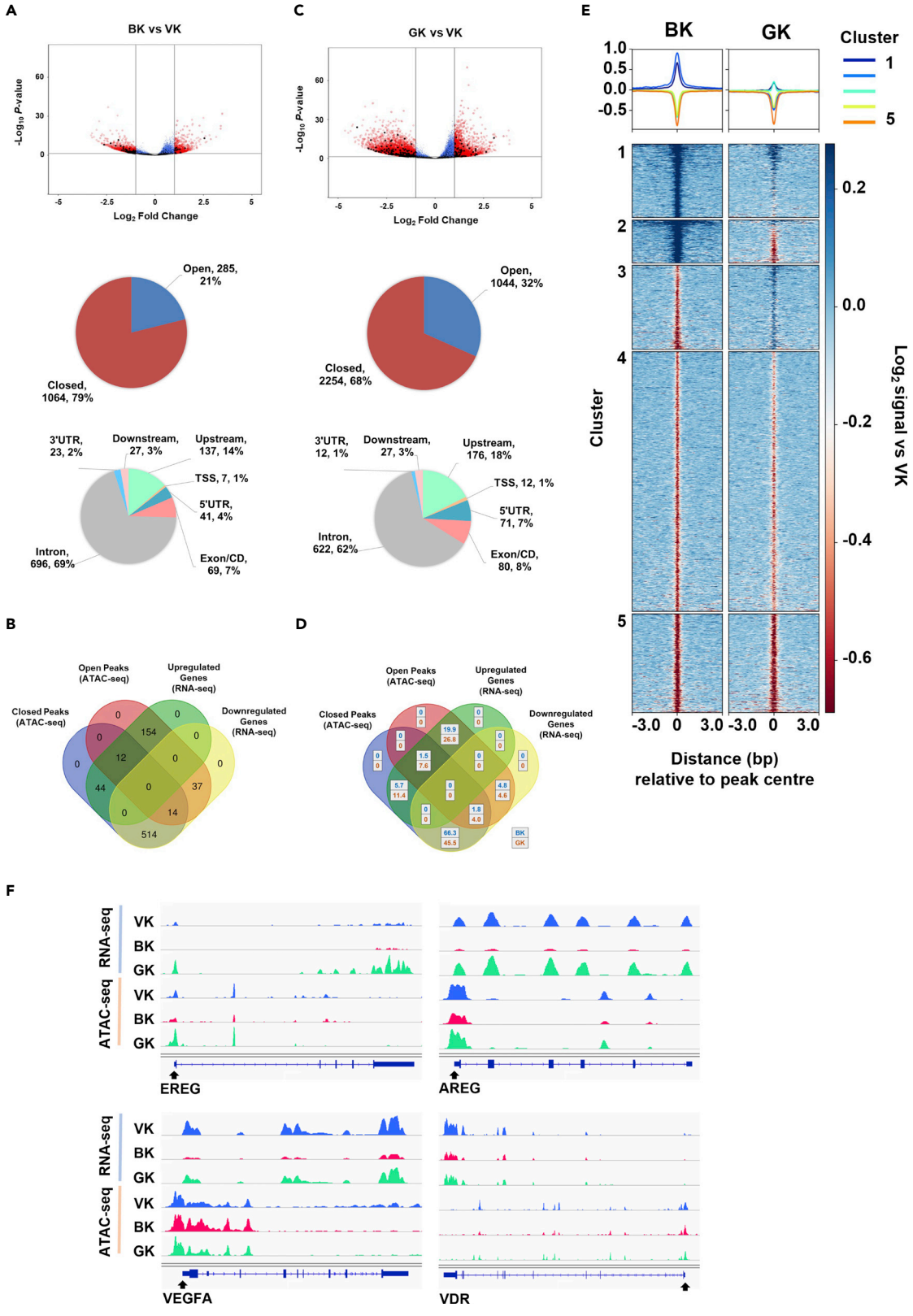
A
BK vs VK
-Log10 P-value
Log2 Fold Change
Open, 285, 21%
Closed, 1064, 79%
3'UTR, 23, 2%
Downstream, 27, 3%
Upstream, 137, 14%
TSS, 7, 1%
5'UTR, 41, 4%
Exon/CD, 69, 7%
Intron, 696, 69%
C
GK vs VK
Open, 1044, 32%
Closed, 2254, 68%
3'UTR, 12, 1%
Downstream, 27, 3%
Upstream, 176, 18%
TSS, 12, 1%
5'UTR, 71, 7%
Exon/CD, 80, 8%
Intron, 622, 62%
E
BK
GK
Cluster
Distance (bp) relative to peak centre
Log2 signal vs VK
B
Open Peaks (ATAC-seq)
Upregulated Genes (RNA-seq)
Closed Peaks (ATAC-seq)
Downregulated Genes (RNA-seq)
D
F
RNA-seq
ATAC-seq
VK
BK
GK
EREG
AREG
VEGFA
VDR

Figure 5. BASP1-dependent modification of chromatin accessibility is mediated by lipidation-dependent and lipidation-independent mechanisms

(A) Volcano plots showing differential analysis of ATAC peaks for BK and GK, vs VK. Peaks overlapping WT1 target genes are shown in black. Open and closed chromatin regions (padj $\leq$0.05 and FC $\geq$ 1 for B-K562 vs V-K562 cells) and their associated genomic features are shown in pie charts. Data are from sequencing of three independently prepared samples. See Table S1 (Quality control analysis of RNA-seq and ATAC-seq data).

(B) Chromatin regions were assigned to the closest gene within 5kb upstream and downstream and are shown (for peaks and genes at padj $\leq$0.05 and FC $\geq$ 1 B-K5623 vs V-K562) as a Venn diagram.

(C) As in part A except that V-K562 and G-K562 cells are compared.

(D) The proportion of open and closed chromatin regions at up and downregulated genes is shown for B-K562 cells and G-K562 cells.

(E) Chromatin regions at padj $\leq$0.05 and fold-change $\geq$ 1 for B-K562 cells vs V-K562 cells are plotted as Log_2 signal vs V-K562 cells for B-K562 cells and G-K562 cells.

(F) Chromatin peaks and gene expression are shown for EREG, AREG, VDR and VEGFA. See also Figures S2 and S3.

Figure 5F shows the comparison of RNA-seq and ATAC-seq analysis across four WT1 target genes, AREG, VDR, EREG, and VEGFA. All four loci show a reduction of RNA-seq signal across the genes in B-K562 cells compared to V-K562 cells, which is coincident with a decrease in the chromatin accessibility around the transcription start sites of each gene (as measured by ATAC-Seq; Figure S3B shows an expanded view with surrounding genomic regions). In G-K562 cells, AREG, VDR, and EREG are not transcriptionally repressed (in-fact, BASP1-G2A activates the transcription of EREG), while VEGFA is still partially repressed by BASP1-G2A. Both EREG and AREG show that BASP1-G2A fails to induce closed ATAC peaks in the vicinity of the transcription start site which is coincident with the failure of BASP1-G2A to repress the transcription of these genes. BASP1-G2A produced an ATAC profile similar to wtBASP1 at the transcription start site region of the VDR gene but instead showed a reduction in ATAC peaks within the main body of the gene. Taken together, these data suggest that BASP1 transcriptionally represses WT1 target genes through the formation of closed chromatin. Furthermore, BASP1-G2A shows gene-specific effects in function, both in the regulation of chromatin compaction and in transcriptional repression.

DISCUSSION

BASP1 represses transcription through a novel mechanism that requires its lipidation to recruit PIP_2 and cholesterol to the promoter region of target genes. The localization of lipids, including PIP_2 and cholesterol, within the nucleus as well as their association with chromatin is well-documented, but their roles in nuclear processes are poorly understood (Garcia-Gil and Albi, 2017; Fernandes et al., 2018; Fiume et al., 2019; Barbosa and Siniossoglou, 2020; Gapa et al., 2022). Here we have presented evidence that myristoylated BASP1 is recruited to the promoter of WT1 target genes. We find that the N-terminal myristoylation of BASP1 controls its ability to modulate the chromatin environment and is needed for the full tumor suppressor activity of BASP1.

We have previously shown that BASP1interacts with PIP_2 to recruit HDAC1 to the gene promoter, which then deacetylates histone H3K9. The enzymes responsible for the BASP1-dependent demethylation of K3K4 and the trimethylation methylation of H3K27 have yet to be identified. It will be interesting to determine if BASP1 recruits the polycomb complex to trimethylate H3K27. BASP1-G2A retains the function to trimethylate H3K27 but is not able to mediate the deacetylation of H3K9 or demethylation of H3K4. This raises the possibility that BASP1-G2A leads to the formation of bivalent histone marks. Bivalent marks are associated with poised promoter regions that can either be activated or repressed (Voigt et al., 2013). The BASP1-G2A mutant derivative still causes significant changes in chromatin accessibility, suggesting that the H3K27 trimethylation function is sufficient, at least for a subset of target genes, to remodel chromatin and alter gene expression. Indeed, our RNAseq data demonstrate that BASP1-G2A retains transcriptional repressor activity at ~46% of WT1 target genes and ~59% overall. Genome-wide analysis of BASP1- and myristoylation-dependent histone modifications could be used to determine if BASP1-G2A leads to the formation of bivalent chromatin. Several previous studies have demonstrated the tumor suppressor activity of BASP1 (Hartl and Schneider, 2019). We found that BASP1-G2A is partially defective in tumor suppressor function which is consistent with the retention of chromatin modification and transcriptional regulatory function. It will be interesting to determine if BASP1 myristoylation plays a similar role in its tumor suppressor activity in other cell types.

The BASP1 G2A mutation prevents terminal myristoylation of BASP1 and abolishes its interaction with lipids. In that respect, the findings presented here raise the question of whether the lipid-binding function of wtBASP1 can be modulated to provide a regulatory mechanism for the transcriptional repression function of BASP1. Indeed, previous studies have demonstrated that the phosphorylation of Serine-6 within

BASP1 generates an unfavorable environment for the binding of lipids by BASP1 (Mosevitsky, 2005). We have previously reported that the phosphorylation of BASP1 disrupts its transcriptional repressor activity (Toska et al., 2012). This raises the possibility that the phosphorylation of BASP1 might regulate its ability to interact with different chromatin remodeling activities in the regulation of the chromatin landscape.

Our RNAseq data suggest that BASP1 can regulate the activity of several transcription factors. These include transcription factors previously identified as partners of BASP1, MYC (Hartl et al., 2009), YY1 (Santiago et al., 2021), and CTCF (Essafi et al., 2011). Several target genes of MYC and the associated MAZ protein were regulated by BASP1 which had both coactivator and corepressor function that was not dependent on the myristoylation of BASP1. This reduced dependence on BASP1 myristoylation might be owing to the proposed alternative mechanism whereby BASP1 interferes with the MYC-Calmodulin interaction. In contrast, YY1 and CTCF target genes showed BASP1-dependent repression that was substantially dependent on BASP1 myristoylation. RELA and TFAP2A/C target genes were also repressed by BASP1 which was dependent on BASP1 myristoylation. Taken together, these results suggest that BASP1 modulates the transcriptional activity of several transcription factors through both lipidation-dependent and lipidation-independent mechanisms.

Limitations of the study

In this study, we evaluated the effect of the disruption of the myristoyl motif of BASP1 on its function as a transcriptional coregulator. As the G2A mutation in BASP1 disrupts the interactions with both PIP_2 and cholesterol, the current study does not discriminate between the contribution of these two lipids to transcriptional regulation. Although we demonstrated that the BASP1-dependent effects on H3K9, H3K4, and H3K237 modification status occur in both K562 cells and in murine taste cells, the genome-wide study was limited to K562 cells. RNAseq and ATACseq in other cell types will be required to confirm the generality of these effects. Further studies to determine the genome-wide localization of BASP1 will be required to distinguish between direct and indirect effects of BASP1 or BASP1 G2A in the RNAseq and ATACseq datasets. Finally, the gene distance cut-off of 10kb that was applied to the analysis of potential regulatory elements is an accepted standard for such analyses, providing a suitable balance of sensitivity and specificity for the detection of *cis*-acting regulatory effects. However, we recognize that this approach excludes distant regulatory elements.

STAR★METHODS

Detailed methods are provided in the online version of this paper and include the following:

- KEY RESOURCES TABLE
- RESOURCE AVAILABILITY
  - Lead contact
  - Materials availability
  - Data and code availability
- METHOD DETAILS
  - Cell lines
  - Chromatin immunoprecipitation
  - qPCR analysis
  - Immunofluorescence
  - Click chemistry
  - Immunoprecipitation
  - Colony formation assay
  - Animals
  - Sample preparation and sequencing
  - RNA-seq and ATAC-seq data analysis
  - Resources and tools
- QUANTIFICATION AND STATISTICAL ANALYSIS

SUPPLEMENTAL INFORMATION

Supplemental information can be found online at https://doi.org/10.1016/j.isci.2022.104796.

ACKNOWLEDGMENTS

This work was funded by the BBSRC so SGER (BB/T001925/1) and NIH to KFM and SGER (1R01GM098609). AEL was supported by a Wellcome Trust PhD Studentship for the Dynamic Cell Biology program (083474). Would like to thank Mutia Muna for her help with the BASP1 mouse experiments.

AUTHOR CONTRIBUTIONS

The study was conceptualized and designed by AJM, AEL, KFM, and SGER. All authors performed experiments and analyzed the data. AJM and SGER wrote the article. All authors discussed the results from the experiments and commented on the article. SGER supervised the project.

DECLARATION OF INTERESTS

The authors declare no competing interests.

INCLUSION AND DIVERSITY

We worked to ensure sex balance in the selection of non-human subjects. While citing references scientifically relevant for this work, we also actively worked to promote gender balance in our reference list.

Received: February 22, 2022
Revised: March 22, 2022
Accepted: July 14, 2022
Published: August 19, 2022

REFERENCES

Ashburner, M., Ball, C.A., Blake, J.A., Botstein, D., Butler, H., Cherry, J.M., Davis, A.P., Dolinski, K., Dwight, S.S., Eppig, J.T., et al. (2000). Gene Ontology: tool for the unification of biology. Nat. Genet. *25*, 25–29. https://doi.org/10.1038/75556.

Barbosa, A.D., and Siniossoglou, S. (2020). New kid on the block: lipid droplets in the nucleus. FEBS J. *287*, 4838–4843. https://doi.org/10.1111/febs.15307.

Blanchard, J.W., Xie, J., El-Mecharrafie, N., Gross, S., Lee, S., Lerner, R.A., and Baldwin, K.K. (2017). Replacing reprogramming factors with antibodies selected from combinatorial antibody libraries. Nat. Biotechnol. *35*, 960–968. https://doi.org/10.1038/nbt.3963.

Blighe, K., Rana, S., and Lewis, M.. EnhancedVolcano: publication-ready volcano plots with enhanced colouring and labelling. https://github.com/kevinblighe/EnhancedVolcano.

Carpenter, B., Hill, K.J., Charalambous, M., Wagner, K.J., Lahiri, D., James, D.I., Andersen, J.S., Schumacher, V., Royer-Pokora, B., Mann, M., et al. (2004). BASP1 is a transcriptional cosuppressor for the Wilms' tumor suppressor protein WT1. Mol. Cell Biol. *24*, 537–549. https://doi.org/10.1128/MCB.24.2.537-549.2004.

Davis, A.P., Grondin, C.J., Johnson, R.J., Sciaky, D., McMorran, R., Wiegers, J., Wiegers, T.C., and Mattingly, C.J. (2019). The comparative toxicogenomics database: update 2019. Nucleic Acids Res. *47*, D948–D954. https://doi.org/10.1093/nar/gky868.

Dobin, A., Davis, C.A., Schlesinger, F., Drenkow, J., Zaleski, C., Jha, S., Batut, P., Chaisson, M., and Gingeras, T.R. (2013). STAR: ultrafast universal RNA-seq aligner. Bioinformatics *29*, 15–21. https://doi.org/10.1093/bioinformatics/bts635.

Draghici, S., Khatri, P., Tarca, A.L., Amin, K., Done, A., Voichita, C., Georgescu, C., and Romero, R. (2007). A systems biology approach for pathway level analysis. Genome Res. *17*, 1537–1545. https://doi.org/10.1101/gr.6202607.

Dutta Banik, D., Martin, L.E., Freichel, M., Torregrossa, A.M., and Medler, K.F. (2018). TRPM4 and TRPM5 are both required for normal signaling in taste receptor cells. Proc. Natl. Acad. Sci. USA *115*, E772–E781. https://doi.org/10.1073/pnas.1718802115.

Epand, R.M. (2008). Proteins and cholesterol-rich domains. Biochim. Biophys. Acta *1778*, 1576–1582. https://doi.org/10.1016/j.bbamem.2008.03.016.

Essafi, A., Webb, A., Berry, R.L., Slight, J., Burn, S.F., Spraggon, L., Velecela, V., Martinez-Estrada, O.M., Wiltshire, J.H., Roberts, S.G., et al. (2011). A wt1-controlled chromatin switching mechanism underpins tissue-specific wnt4 activation and repression. Dev. Cell *21*, 559–574. https://doi.org/10.1016/j.devcel.2011.07.014.

Fernandes, V., Teles, K., Ribeiro, C., Treptow, W., and Santos, G. (2018). Fat nucleosome: role of lipids on chromatin. Prog. Lipid Res. *70*, 29–34. https://doi.org/10.1016/j.plipres.2018.04.003.

Fiume, R., Faenza, I., Sheth, B., Poli, A., Vidalle, M.C., Mazzetti, C., Abdul, S.H., Campagnoli, F., Fabbrini, M., Kimber, S.T., et al. (2019). Nuclear phosphoinositides: their regulation and roles in nuclear functions. Int. J. Mol. Sci. *20*, E2991. https://doi.org/10.3390/ijms20122991.

Gapa, L., Alfardus, H., and Fischle, W. (2022). Unconventional metabolites in chromatin regulation. Biosci. Rep. *42*. BSR20211558. https://doi.org/10.1042/BSR20211558.

Gaspar, J.M. (2018). Improved peak-calling with MACS2. Preprint at bioRxiv. 496521. https://doi.org/10.1101/496521.

Gao, Y., Toska, E., Denmon, D., Roberts, S.G., and Medler, K.F. (2014). WT1 regulates the development of the posterior taste field. Development *141*, 2271–2278. https://doi.org/10.1242/dev.105676.

Gao, Y., Dutta Banik, D., Muna, M.M., Roberts, S.G., and Medler, K.F. (2019). The WT1-BASP1 complex is required to maintain the differentiated state of taste receptor cells. Life Sci. Alliance *2*, e201800287. https://doi.org/10.26508/lsa.201800287.

Garcia-Gil, M., and Albi, E. (2017). Nuclear lipids in the nervous system: what they do in health and disease. Neurochem. Res. *42*, 321–336. https://doi.org/10.1007/s11064-016-2085-8.

Goodfellow, S.J., Rebello, M.R., Toska, E., Zeef, L.A., Rudd, S.G., Medler, K.F., and Roberts, S.G. (2011). WT1 and its transcriptional cofactor BASP1 redirect the differentiation pathway of an established blood cell line. Biochem. J. *435*, 113–125. https://doi.org/10.1042/BJ20101734.

Hartl, M., and Schneider, R. (2019). A unique family of neuronal signaling proteins implicated in oncogenesis and tumor suppression. Front. Oncol. *9*, 289. https://doi.org/10.3389/fonc.2019.00289.

Hartl, M., Nist, A., Khan, M.I., Valovka, T., and Bister, K. (2009). Inhibition of Myc-induced cell transformation by brain acid-soluble protein 1 (BASP1). Proc. Natl. Acad. Sci. USA *106*, 5604–5609. https://doi.org/10.1073/pnas.0812101106.

Huang, W., Loganantharaj, R., Schroeder, B., Fargo, D., and Li, L. (2013). PAVIS: a tool for peak annotation and visualization. Bioinformatics *29*,

3097–3099. https://doi.org/10.1093/bioinformatics/btt520.

Kanehisa, M., Goto, S., Sato, Y., Furumichi, M., and Tanabe, M. (2012). KEGG for integration and interpretation of large-scale molecular data sets. Nucleic Acids Res. *40*, 109–114. https://doi.org/10.1093/nar/gkr988.

Kolde, R. (2019). pheatmap. https://github.com/raivokolde/pheatmap.

Kozomara, A., Birgaoanu, M., and Griffiths-Jones, S. (2019). MiRBase: from microRNA sequences to function. Nucleic Acids Res. *47*, D155–D162. https://doi.org/10.1093/nar/gky1141.

Li, H., and Durbin, R. (2009). Fast and accurate short read alignment with Burrows-Wheeler transform. Bioinformatics *25*, 1754–1760. https://doi.org/10.1093/bioinformatics/btp324.

Li, L., Meng, Q., Li, G., and Zhao, L. (2020). BASP1 suppresses cell growth and metastasis through inhibiting wnt/beta-catenin pathway in gastric cancer. BioMed Res. Int. *2020*, 8628695. https://doi.org/10.1155/2020/8628695.

Liao, Y., Smyth, G.K., and Shi, W. (2013). The Subread aligner: fast, accurate and scalable read mapping by seed-and-vote. Nucleic Acids Res. *41*, e108. https://doi.org/10.1093/nar/gkt214.

Linde, N., and Stick, R. (2010). Intranuclear membranes induced by lipidated proteins are derived from the nuclear envelope. Nucleus *1*, 343–353. https://doi.org/10.4161/nucl.1.4.12352.

Loats, A.E., Carrera, S., Fleming, A.F., Roberts, A.R.E., Sherrard, A., Toska, E., Moorhouse, A.J., Medler, K.F., and Roberts, S.G.E. (2021). Cholesterol is required for transcriptional repression by BASP1. Proc. Natl. Acad. Sci. USA *118*. e2101671118. https://doi.org/10.1073/pnas.2101671118.

Love, M.I., Huber, W., and Anders, S. (2014). Moderated estimation of fold change and dispersion for RNA-seq data with DESeq2. Genome Biol. *15*, 1–21. https://doi.org/10.1186/s13059-014-0550-8.

Marsh, L.A., Carrera, S., Shandilya, J., Heesom, K.J., Davidson, A.D., Medler, K.F., and Roberts, S.G. (2017). BASP1 interacts with oestrogen receptor α and modifies the tamoxifen response. Cell Death Dis. *8*, e2771. https://doi.org/10.1038/cddis.2017.179.

McGeary, S.E., Lin, K.S., Shi, C.Y., Pham, T.M., Bisaria, N., Kelley, G.M., and Bartel, D.P. (2019). The biochemical basis of microRNA targeting efficacy. Science *366*, eaav1741. https://doi.org/10.1126/science.aav1741.

McLean, C.Y., Bristor, D., Hiller, M., Clarke, S.L., Schaar, B.T., Lowe, C.B., Wenger, A.M., and Bejerano, G. (2010). GREAT improves functional interpretation of cis-regulatory regions. Nat. Biotechnol. *28*, 495–501. https://doi.org/10.1038/nbt.1630.

Mosevitsky, M.I. (2005). Nerve ending "signal" proteins GAP-43, MARCKS, and BASP1. Int. Rev. Cytol. *245*, 245–325. https://doi.org/10.1016/S0074-7696(05)45007-X.

Ramírez, F., Ryan, D.P., Grüning, B., Bhardwaj, V., Kilpert, F., Richter, A.S., Heyne, S., Dündar, F., and Manke, T. (2016). deepTools2: a next generation web server for deep-sequencing data analysis. Nucleic Acids Res. *44*, W160–W165. https://doi.org/10.1093/nar/gkw257.

Raudvere, U., Kolberg, L., Kuzmin, I., Arak, T., Adler, P., Peterson, H., and Vilo, J. (2019). G:Profiler: a web server for functional enrichment analysis and conversions of gene lists (2019 update). Nucleic Acids Res. *47*, W191–W198. https://doi.org/10.1093/nar/gkz369.

Santiago, F.S., Li, Y., Zhong, L., Raftery, M.J., Lins, L., and Khachigian, L.M. (2021). Truncated YY1 interacts with BASP1 through a 339KLK341 motif in YY1 and suppresses vascular smooth muscle cell growth and intimal hyperplasia after vascular injury. Cardiovasc. Res. *117*, 2395–2406. https://doi.org/10.1093/cvr/cvab021.

Schneider, C.A., Rasband, W.S., and Eliceiri, K.W. (2012). NIH Image to ImageJ: 25 years of image analysis. Nat. Methods *9*, 671–675.

Szklarczyk, D., Morris, J.H., Cook, H., Kuhn, M., Wyder, S., Simonovic, M., Santos, A., Doncheva, N.T., Roth, A., Bork, P., et al. (2017). The STRING database in 2017: quality-controlled protein-protein association networks, made broadly accessible. Nucleic Acids Res. *45*, D362–D368. https://doi.org/10.1093/nar/gkw937.

Tarca, A.L., Draghici, S., Khatri, P., Hassan, S.S., Mittal, P., Kim, J.S., Kim, C.J., Kusanovic, J.P., and Romero, R. (2009). A novel signaling pathway impact analysis. Bioinformatics *25*, 75–82. https://doi.org/10.1093/bioinformatics/btn577.

Thorvaldsdóttir, H., Robinson, J.T., and Mesirov, J.P. (2013). Integrative Genomics Viewer (IGV): high-performance genomics data visualization and exploration. Brief. Bioinform. *14*, 178–192. https://doi.org/10.1093/bib/bbs017.

Toska, E., Campbell, H.A., Shandilya, J., Goodfellow, S.J., Shore, P., Medler, K.F., and Roberts, S.G.E. (2012). Repression of transcription by WT1-BASP1 requires the myristoylation of BASP1 and the PIP2-dependent recruitment of histone deacetylase. Cell Rep. *2*, 462–469. https://doi.org/10.1016/j.celrep.2012.08.005.

Toska, E., and Roberts, S.G.E. (2014). Mechanisms of transcriptional regulation by WT1 (Wilms' tumour 1). Biochem. J. *461*, 15–32. https://doi.org/10.1042/BJ20131587.

Toska, E., Shandilya, J., Goodfellow, S.J., Medler, K.F., and Roberts, S.G.E. (2014). Prohibitin is required for transcriptional repression by the WT1-BASP1 complex. Oncogene *33*, 5100–5108. https://doi.org/10.1038/onc.2013.447.

Tsunedomi, R., Ogawa, Y., Iizuka, N., Sakamoto, K., Tamesa, T., Moribe, T., and Oka, M. (2010). The assessment of methylated BASP1 and SRD5A2 levels in the detection of early hepatocellular carcinoma. Int. J. Oncol. *36*, 205–212. https://doi.org/10.3892/ijo_00000491.

Voigt, P., Tee, W.W., and Reinberg, D. (2013). A double take on bivalent promoters. Genes Dev. *27*, 1318–1338. https://doi.org/10.1101/gad.219626.113.

Wickham, H. (2016). ggplot2: Elegant Graphics for Data Analysis (Springer-Verlag), ISBN 978-3-319-24277-4, https://ggplot2.tidyverse.org.

Wright, M.H., Paape, D., Storck, E.M., Serwa, R.A., Smith, D.F., and Tate, E.W. (2015). Global analysis of protein N-myristoylation and exploration of N-myristoyltransferase as a drug target in the neglected human pathogen Leishmania donovani. Chem. Biol. *22*, 342–354. https://doi.org/10.1016/j.chembiol.2015.01.003.

STAR★METHODS

KEY RESOURCES TABLE

REAGENT or RESOURCE	SOURCE	IDENTIFIER
Antibodies		
Normal rabbit IgG	Merck-Millipore	Cat#12–379; RRID:AB_145841
Normal mouse IgG	Merck-Millipore	Cat#12–371; RRID:AB_145840
Rabbit polyclonal anti H3K4me3	Merck-Millipore	Cat#07–473; RRID:AB_1977252
Rabbit polyclonal anti H3K9Ac	Abcam	Cat#ab10812; RRID:AB_297491
Rabbit polyclonal anti-K3K27me3	Abcam	Cat#ab6002; RRID: AB_305237
Mouse monoclonal anti-RNA polymerase II	Abcam	Cat#ab 817; RRID:AB_306327
Mouse monoclonal anti-β-actin	Sigma-Aldrich	Cat#A5316; RRID:AB_476743
Rabbit polyclonal anti-BASP1	Carpenter et al. (2004)	https://doi.org/10.1128/mcb.24.2.537-549.2004
Rabbit polyclonal anti-WT1	Gao et al. (2019)	https://doi.org/10.26508/lsa.201800287
Rabbit polyclonal β-tubulin	Abcam	Cat# ab6046; RRID:AB_2210370
Anti-Mouse-HRP	Merck-Millipore	Cat#71045-3; RRID: AB_10808067
Anti-Rabbit-HRP	Merck-Millipore	Cat#AP304P; RRID: AB_11212320
Chemicals, peptides, and recombinant proteins		
Streptavidin, Alexa Fluor™ 594 Conjugate	ThermoFisher	Cat# S32356
Alkyne myristic acid	Cayman Chemical	Cat# 13267
Azide-PEG3-biotin conjugate	Sigma-Aldrich	Cat# 762024
Streptavidin magnetic beads	ThermoFisher	Cat# 88816
Protein G magnetic beads	ThermoFisher	Cat# 88847
G-418	Sigma-Aldrich	Cat# A1720
Immobilon-P PVDF Membrane	Merck-Millipore	Cat# IPVH00010
RPMI 1640 medium	ThermoFisher	Cat# 11875101
Penicillin/Streptomycin	Sigma-Aldrich	Cat# P4333
L-Glutamine	Sigma-Aldrich	Cat# G7513
Protease inhibitor cocktail	Merck-Millipore	Cat# 539131
Proteinase K	Ambion	Cat# AM2546
DAPI solution	ThermoFisher	Cat# 62248
DABCO mounting medium	Sigma-Aldrich	Cat# 290734
Effectene transfection reagent	Qiagen	Cat# 301425
Tamoxifen	Sigma-Aldrich	Cat# T5648
Critical commercial assays		
Nuclei EZ prep	Sigma-Aldrich	Cat# NUC101-1KT
RNeasy mini kit	Qiagen	Cat#74104
QIAprep Spin Miniprep Kit	Qiagen	Cat# 27104
QIAquick PCR Purification Kit	Qiagen	Cat# 28104
iScript cDNA synthesis kit	Bio-Rad	Cat# 1708890
iTaq Universal Sybr Green Supermix	Bio-Rad	Cat# 1725121
Deposited data		
RNA-Seq data	GEO	GSE196525
ATAC-Seq data	GEO	GSE196525

(*Continued on next page*)

Continued

REAGENT or RESOURCE	SOURCE	IDENTIFIER
Experimental models: Cell lines		
K562	ECACC	Cat# 89121407 RRID:CVCL_0004
V-K562	Goodfellow et al. (2011)	https://doi.org/10.1042/BJ20101734
B-K562	Goodfellow et al. (2011)	https://doi.org/10.1042/BJ20101734
G-K562	Toska et al. (2012)	doi:10.1016/j.celrep.2012.08.005
Experimental models: Organisms/strains		
Floxed BASP1 mouse	Gao et al. (2019)	doi:10.26508/lsa.201800287
Krt8-Cre/ERT2+ mouse	The Jackson Laboratory: Strain #:017947	RRID:IMSR_JAX:017947
Oligonucleotides		
Human AREG cDNA Forward	IDT	TGGATTGGACCTCAATGACA
Human AREG cDNA Reverse	IDT	ACTGTGGTCCCCAGAAAATG
Human VDR cDNA Forward	IDT	CTGACCCTGGAGACTTTGAC
Human VDR cDNA Reverse	IDT	TTCCTCTGCACTTCCTCAT
Human GAPDH cDNA Forward	IDT	ACAGTCAGCCGCATCTTCTT
Human GAPDH cDNA Reverse	IDT	ACGACCAAATCCGTTGACTC
Human AREG ChIP Forward	IDT	TTTAAGTTCCACTTCCTCTCA
Human AREG ChIP Reverse	IDT	GGTGTGCGAACGTCTGTA
Human VDR ChIP Forward	IDT	CACCTGGCTCAGGCGTCC
Human VDR ChIP Reverse	IDT	GCCAGGAGCTCCGTTGGC
Human BAX (Ctrl) ChIP Forward	IDT	CAGCTCAGTGCTGTTGGTGG
Human BAX (Ctrl) ChIP Reverse	IDT	ACCATCCAACCCTGGAGATC
18S (Ctrl) ChIP Forward	IDT	GTAACCCGTTGAACCCCATT
18S (Ctrl) ChIP Reverse	IDT	CCATCCAATCGGTAGTAGCG
Mouse floxed BASP1-genotyping Forward	IDT	TGCCCTGCCTGCAGGTCAAT
Mouse floxed BASP1-genotyping Reverse	IDT	CCGAGTCTGTACAAAAGCCACC
Mouse BASP1 cDNA Forward	IDT	CTTTCAGACGGAGCCCACTT
Mouse BASP1 cDNA Reverse	IDT	AACTACAGGTGCACCCAACC
Mouse LEF1 cDNA Forward	IDT	CCCACACGGACAGTGACCTA
Mouse LEF1 cDNA Reverse	IDT	TGGGCTCCTGCTCCTTTCT
Mouse PTCH1 cDNA Forward	IDT	TTTCCAAGGGGAAGGCTACT
Mouse PTCH1 cDNA Reverse	IDT	CTTTAATCCCACAGCGAAGG
Mouse LEF1 ChIP Forward	IDT	TCAGTCATCCCGAAGAGGAG
Mouse LEF1 ChIP Reverse	IDT	GCCACCGTTTAGCCATAGAA
Mouse PTCH1 ChIP Forward	IDT	CCGAAGATTTAAGGTGGCAA
Mouse PTCH1 ChIP Reverse	IDT	GGAGGGAGCCAAAGTAAAGG
Mouse Control ChIP Forward	IDT	TTCCGAGGGTTGTGAGAACG
Mouse Control ChIP Reverse	IDT	GGATCCCCCTAGAGAAGGCT
Software and algorithms		
Image J	Schneider et al., 2012	https://imagej.nih.gov/ij/
Volocity 6.3	Quorum Technologies	quorumtechnologies.com
CFX Manager (MiniOpticon) Version 3	Bio-Rad	Cat# 1845003
OriginPro 7.5	OriginLab	Originlab.com
STAR	Dobin et al. (2013)	https://github.com/alexdobin/STAR
BWA-mem	Li and Durbin (2009)	https://github.com/lh3/bwa
Subread	Liao et al. (2013)	http://subread.sourceforge.net/

(*Continued on next page*)

Continued

REAGENT or RESOURCE	SOURCE	IDENTIFIER
MACS2	Gaspar (2018)	https://hbctraining.github.io/Intro-to-ChIPseq/lessons/05_peak_calling_macs.html
DESeq2	Love et al. (2014)	https://bioconductor.org/packages/release/bioc/html/DESeq2.html
IGV	Thorvaldsdóttir et al. (2013)	https://github.com/igvteam/igv
iPathway	Draghici et al. (2007)	https://advaitabio.com/ipathwayguide/
deepTools2	Ramírez et al. (2016)	https://github.com/deeptools/deepTools
pheatmap	Kolde (2019)	https://github.com/raivokolde/pheatmap
EnhancedVolcano	Blighe et al. (2021)	https://github.com/kevinblighe/EnhancedVolcano
ggplot2	Wickham (2016)	https://github.com/tidyverse/ggplot2
Pavis2	Huang et al. (2013)	https://manticore.niehs.nih.gov/pavis2/
GREAT	McLean et al. (2010)	http://great.stanford.edu/public/html/
g:Profiler	Raudvere et al. (2019)	https://biit.cs.ut.ee/gprofiler/gost

RESOURCE AVAILABILITY

Lead contact

Further information and requests for resources and reagents should be directed to and will be fulfilled by the Lead Contact, Stefan Roberts (Stefan.Roberts@bristol.ac.uk).

Materials availability

This study did not generate unique reagents.

Data and code availability

All data reported in this paper will be shared by the lead contact upon request. The RNA-seq and ATAC-seq data are available at the NCBI Gene Expression Omnibus GSE196525. This paper does not report original code. Any additional information required to reanalyze the data reported in this paper is available from the lead contact upon request.

METHOD DETAILS

Cell lines

K562 cells, derived from a pleural effusion of 53 year old female with chronic myelogenous leukemia in terminal blast crisis (ECACC), were maintained in RPMI 1640 (ThermoFisher) supplemented with 10% (v/v) fetal calf serum (Sigma-Aldrich), 1% (v/v) Pen-Strep (Sigma-Aldrich) and 1% (v/v) L-glutamine (Sigma-Aldrich). Stably transfected K562 cell line derivatives selected as a pool (Goodfellow et al., 2011; Toska et al., 2012) were supplemented with 1 mg/mL G-418 (Sigma-Aldrich). All cell line derivatives were screened by immunofluorescence to ensure that BASP1 was expressed in >95% of the cells. Cells were incubated at 37°C in humidified 95% air and 5% CO_2. Lipid-free media was prepared as above but using charcoal-stripped fetal calf serum (Thermofisher).

Chromatin immunoprecipitation

K562 cells were harvested and resuspended to a density of 1×10^6 cells/mL in PBS. Crosslinking was initiated by the addition of formaldehyde to a final concentration of 1.42% (v/v) and incubation at room temperature for 15 min. Crosslinking was terminated by the addition of glycine to a final concentration of 125mM glycine and incubation at 4°C for 5 min. The cells were then harvested by centrifugation at 2000 x g for 5 min at 4°C and then washed with PBS. Cells were resuspended and lysed in 1mL IP buffer (150mM NaCl, 50mM Tris-HCl (pH 7.5), 5mM EDTA, 0.5% (v/v) NP-40 and 1% (v/v) Triton X-100) with protease inhibitor cocktail for 15 min on ice. After centrifugation at 2000 x g for 5 min at 4°C, the pellet resuspended in 1mL IP buffer. The chromatin was sheared by sonication using a QSonica Q500 at 60% amplitude and the lysate was cleared by centrifugation at 12000 x g for 10 min at 4°C. The samples were pre-cleared by

incubation for 1 h at 4°C on a rotator with 10μL Protein G magnetic beads (ThermoFisher). The indicated antibody was incubated in 600μL IP buffer containing 1μL 10 mg/mL acetylated BSA and 5μL Protein G magnetic beads for 4 h with rotation at 4°C. 200μL of the pre-cleared chromatin was added and incubation continued at 4°C overnight. A sample of the input chromatin was stored for later decrosslinking and processing.

After incubation, the samples were collected on a magnetic rack and beads sequentially washed once in IP buffer, high salt IP buffer (500mM NaCl, 50mM Tris-HCl (pH 8.0), 5mM EDTA, 0.5% (v/v) NP-40, 1% (v/v) Triton X-100), LiCl buffer (10mM Tris-HCl (pH 8.0), 250mM LiCl, 1mM EDTA, 1% (v/v) NP-40, 1% (w/v) Sodium Deoxycholate), and TE buffer (10mM Tris-HCl (pH 8.0), 1mM EDTA). The beads were then resuspended in 100μL of PK buffer (125mM Tris-HCl (pH 8.0), 10mM EDTA, 150mM NaCl, 1% (w/v) SDS) and incubated at 65°C overnight. 1μL of 20 mg/mL Proteinase K fwas then added and the samples incubated for at 55°C for 4 h. The immunoprecipitated DNA was finally purified using the Qiaquick PCR purification kit (Qiagen).

qPCR analysis

Total RNA was prepared using the RNeasy kit (Qiagen) and then cDNA prepared using the Iscript cDNA synthesis kit (Bio-Rad). qPCR was performed in triplicate using the iQ SYBR green master mix (Bio-Rad) on a Bio-Rad Miniopticon system. ChIP analysis was performed using promoter-specific primers as indicated and fold-enrichment calculated against a control genomic region. Melt curve analysis was performed at the end of each run. Data were collected using the BioRad-CFX Manager software. The relative expression of each target gene is expressed relative to control GAPDH. Data are expressed as mean with SD(SDM). Data distribution and significance between different groups was analyzed in Excel or OriginPro 7.5 using Student's t test.

Immunofluorescence

K562 cell line derivatives were collected by centrifugation at 1400 x g for 3 min and nuclei were isolated using the Nuclei EZ Prep nuclei isolation kit (Sigma-Aldrich). The nuclei were fixed in 4% (v/v) paraformaldehyde at room temperature for 15 min, then incubated with 50mM NH_4Cl for 15 min with rotation. The fixed nuclei were then washed three times in PBS and then incubated in blocking buffer (2% (w/v) BSA, 0.25% (w/v) Gelatin, 0.2% (w/v) Glycine, 0.2% (v/v) Triton X-100 in PBS) for 1 h with rotation at room temperature. Primary antibody was added to each sample of nuclei in PBS containing 1% (w/v) BSA, 0.25% (w/v) gelatin and 0.2% (v/v) Triton X-100 and then incubated for 1 h with rotation at room temperature. The nuclei were then washed three times with washing buffer (0.2% (w/v) Gelatin in PBS). Fluorescent secondary antibody in PBS containing 1% (w/v) BSA, 0.25% (w/v) gelatin and 0.2% (v/v) Triton X-100 was then incubated with the nuclei for 45 min in with rotation in the dark. After washing three times the samples were incubated with DAP solution for 10 min and then resuspended in a minimum volume of DABCO mounting media (Sigma-Aldrich) an applied to poly-lysine coated slides. Nuclei were viewed using a Leica SP5-II AOBS confocal laser scanning microscope attached to a Leica DM I6000 inverted epifluorescence microscope with oil 63x lens. Images were processed using ImageJ or Volocity 6.3 software.

Click chemistry

K-562 cells were incubated in lipid free media containing 10 μg/mL myristic acid-alkyne (Avanti) for 16 h. Cells were then harvested and washed once in PBS and the nuclei isolated using the EZ Prep nuclei kit. The purified nuclei were then incubated with 50μM Azide-PEG3-biotin conjugate (Sigma-Aldrich) in Buffer A and added to samples. The click reaction was initiated via addition of 2mM CuBF4 in 2% (v/v) acetonitrile, and the reaction was left to proceed at 43°C for 30 min with rotation. The nuclei were then washed in 0.1M HEPES/KOH (pH 7.4) and immediately used for either preparation of nuclear extract for immunoprecipitation, chromatin immunoprecipitation or immunofluorescence.

Immunoprecipitation

Following completion of the click chemistry reaction, nuclear extracts were prepared by resuspending samples in one PCV of NE2 buffer (20 mM HEPES pH 8.0, 1.5 mM MgCl2, 25% (v/v) Glycerol, 420 mM NaCl, 0.2 mM EDTA, 1 mM DTT and 0.5 mM PMSF) and incubating on ice with regular stirring for 30 min. Nuclear debris was pelleted by 5 min in a microfuge at full speed. The cleared nuclear extracts were then subjected to immunoprecipitation using streptavidin magnetic beads (Invitrogen) and IP buffer (20 mM HEPES pH 8.0,

100 mM KCl, 0.2 mM EDTA, 20% (v/v) Glycerol, 0.5 mM DTT and 0.05% (v/v) NP-40) overnight at 4°C. Magnetic beads were collected and washed 3 times in IP buffer.

Colony formation assay

The K562 cell line derivatives were seeded onto agar bases (0.7% (w/v) LMP Agarose, 10% (v/v) FBS, 1% (v/v) Pen Strep, 1% (v/v) L-glutamine in DMEM media supplemented with 0.15% (v/v) NaHCO3, 200 μM sodium pyruvate and 800 μM NaOH at a density of 2 × 105 cells per mL of agar. Agar dishes were fed with additional agar (2 mL) on days 7 and 14 post seeding. The colony formation efficiency (%CFE) was calculated 7, 14 and 21 days post seeding via counting colonies consisting of greater than 50 cells, in a minimum of ten 15.89 mm^2 fields of view per 60 mm^2 dish. Average colony area was measured using ImageJ software. All experiments were performed in triplicate.

Animals

The floxed BASP1 mice in a C57BL/6 background have been described before (Gao et al., 2019). We have not detected any sex differences related to the effects of BASP1 loss. However, we routinely kept records of both sex and age (2–5 months) to ensure no bias is introduced. Animals were cared for in compliance with the University at Buffalo Animal Care and Use Committee. BASP1fl+/− mice were mated with Krt8-Cre/ERT2+ mice (The Jackson Laboratory) to obtain BASP1fl+/−Krt8-Cre/ERT2+ mice and then bred to obtain BASP1fl+/+Krt8-Cre/ERT2+ mice. BASP1fl−/−; Krt8-Cre/ERT2+ or BASP1fl+/+; Krt8-Cre/ERT2− littermates were used as wild-type controls. Adult mice were gavaged with 100 mg/kg body weight of Tamoxifen dissolved in corn oil/ethanol (9:1 by volume) daily for 8 days 7 days later the mice were euthanized and taste receptor cells harvested from the circumvallate papillae as described before (Dutta Banik et al., 2018). The mice were euthanized by carbon dioxide followed by cervical dislocation and the tongues removed. A solution containing 0.7 mg/mL Collagenase B (Roche), 3 mg/mL Dispase II (Roche), and 1 mg/mL trypsin inhibitor (Sigma-Aldrich) was then injected beneath the lingual epithelium. The tongues were then incubated in in oxygenated Tyrode's solution for 15 min and then the epithelium peeled from the muscle and placed in Ca2+-free Tyrode's. The cells were used immediately for either RNA preparation or ChIP.

Sample preparation and sequencing

All samples were prepared in biological triplicates for V-K562, B-K562 and G-K562 cells harvested at 0.7–0.8 × 10^6 cells/mL (Loats et al., 2021; Toska et al., 2012). Cells taken for ATAC-seq were treated with DNase and incubated for 30 mins buffered with 25mM MgCl2 and 5mM CaCl2 prior to harvesting. Samples of 2 × 10^6 for RNA-seq and of 1 × 10^5 cells for ATAC-seq were then pelleted and snap-frozen in liquid nitrogen until library preparation. Total RNA was isolated from the cells using the RNeasy Mini Kit (Qiagen, cat 74104), RNA Integrity Number (RIN) was determined for each sample using Tape Station 4150 System (Agilent). Libraries were prepared according to manufacturer's instructions for TruSeq Stranded mRNA Library kit (Illumina, cat #20020594) and ATAC-Seq Kit (Active Motif, cat #53150). Libraries were sequenced on Illumina NextSeq 500 in 75-nt (RNA-seq) and 42-nt (ATAC-seq) experiments in paired-end mode.

RNA-seq and ATAC-seq data analysis

Reads were mapped to GRCh38 human reference genome using STAR(Dobin et al., 2013) (RNA-seq) and BWA-MEM(Li and Durbin, 2009) (ATAC-seq), duplicate reads were removed, uniquely mapping reads with ≤2 mismatches were kept for downstream analysis. RNA-seq paired reads were assigned to RefSeq transcripts using Subread and annotated with Entrez gene identifiers. ATAC peaks were called using MACS2, merged regions were defined by overlapping intervals between all samples, peak fragment densities for merged regions were used for comparative analysis and annotated with the closest gene within a 10kb window. DESeq2 was used for differential expression analysis to determine p-adjusted values (padj) and shrunken Log2 fold-change (FC) for RNA-seq genes and ATAC-seq merged regions.(Gaspar, 2018; Liao et al., 2013; Love et al., 2014)

The 5000 most differentially expressed genes for BK vs VK at padj ≤0.05 were analyzed using iPathway to determine significantly differentially regulated networks. The 'Impact Analysis' was applied to underlying pathway topologies comprised of genes and their directional interactions. The probability of observing the number of DE genes in a given pathway that is ≥ to that observed by random chance (pORA) and perturbation accumulation, based on the combined perturbation of all genes within the pathway as a function of normalised change in expression and weighting in relation to gene type, (pAcc), are the principal measures

of pathway enrichment. The prediction of upstream regulators is based on the enrichment of differentially expressed genes within networks of regulatory interactions, briefly, each upstream regulator *u*, the number of consistent DE genes downstream of *u*, DTI(u) is compared to the number of measured target genes expected to be both consistent and DE by chance. The *Z* score P_z is the one-tailed area under the probability density function for a normal distribution, N(0,1), P_n is based on the number of DE targets consistent with inhibition.(Draghici et al., 2007; Tarca et al., 2009).

Resources and tools

The following resources were used in pathway enrichment analysis. Gene Ontology Consortium database (as at Oct 2020) (Ashburner et al., 2000). TARGETSCAN (v7.2) (McGeary et al., 2019). miRBase (v22.1, 2020) (Kozomara et al., 2019). KEGG database (v96.0, 2020) (Kanehisa et al., 2012). Comparative Toxicogenomics Database (as at Jul 2020) (Davis et al., 2019). BioGRID: Biological General Repository for Interaction Datasets (v4.0.189, 2020) (Szklarczyk et al., 2017).

Heatmaps were produced from RNA-seq scaled read counts using pheatmap (https://github.com/raivokolde/pheatmap), and from ATAC-seq bigwig signals, log2 normalised for BK and GK against VK, using deepTools2 (https://github.com/deeptools/deepTools) (Ramírez et al., 2016). Volcano plots were produced using EnhancedVolcano (https://github.com/kevinblighe/EnhancedVolcano). Additional plots were prepared with ggplot2 (https://github.com/tidyverse/ggplot2). Pavis2 (https://manticore.niehs.nih.gov/pavis2/) (Huang et al., 2013) and GREAT (http://great.stanford.edu/public/html/) (McLean et al., 2010) were used with default settings for annotations. g:Profiler (https://biit.cs.ut.ee/gprofiler/gost) (Raudvere et al., 2019) was used to explore gene set functional annotations. The Harmonizome (https://maayanlab.cloud/Harmonizome/) databases were used for exploration of transcription factors and their targets. IGV was used to capture genome browser views (https://github.com/igvteam/igv) (Thorvaldsdóttir et al., 2013).

QUANTIFICATION AND STATISTICAL ANALYSIS

Data are expressed as mean with SD(SDM). The Student's t-test was used to compare differences between samples analyzed and p values of less than 0.05 were considered as statistically significant. *: $p < 0.05$, **: $p < 0.01$, ***: $p < 0.001$. Number of biological repeats is indicated in the figure legends.